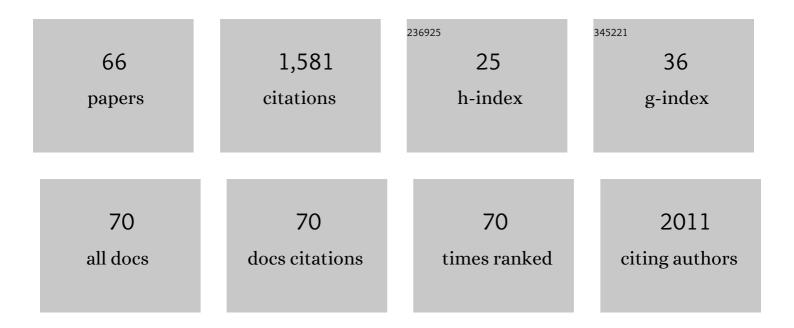
Francesco Iacoviello

List of Publications by Year in descending order

Source: https://exaly.com/author-pdf/8887180/publications.pdf Version: 2024-02-01



#	Article	IF	CITATIONS
1	Antarctic ice sheet sensitivity to atmospheric CO ₂ variations in the early to mid-Miocene. Proceedings of the National Academy of Sciences of the United States of America, 2016, 113, 3453-3458.	7.1	133
2	Quantifying the anisotropy and tortuosity of permeable pathways in clay-rich mudstones using models based on X-ray tomography. Scientific Reports, 2017, 7, 14838.	3.3	97
3	Investigation of Hot Pressed Polymer Electrolyte Fuel Cell Assemblies via X-ray Computed Tomography. Electrochimica Acta, 2017, 242, 125-136.	5.2	74
4	Aqueous Inks of Pristine Graphene for 3D Printed Microsupercapacitors with High Capacitance. ACS Nano, 2021, 15, 15342-15353.	14.6	60
5	Laserâ€preparation of geometrically optimised samples for Xâ€ray nanoâ€CT. Journal of Microscopy, 2017, 267, 384-396.	1.8	54
6	The effect of non-uniform compression and flow-field arrangements on membrane electrode assemblies - X-ray computed tomography characterisation and effective parameter determination. Journal of Power Sources, 2019, 426, 97-110.	7.8	46
7	Novel laboratory investigation of huff-n-puff gas injection for shale oils under realistic reservoir conditions. Fuel, 2021, 284, 118950.	6.4	43
8	In situ compression and X-ray computed tomography of flow battery electrodes. Journal of Energy Chemistry, 2018, 27, 1353-1361.	12.9	42
9	Correlative study of microstructure and performance for porous transport layers in polymer electrolyte membrane water electrolysers by X-ray computed tomography and electrochemical characterization. International Journal of Hydrogen Energy, 2019, 44, 19519-19532.	7.1	41
10	Enhanced primary productivity and magnetotactic bacterial production in response to middle Eocene warming in the Neo-Tethys Ocean. Palaeogeography, Palaeoclimatology, Palaeoecology, 2014, 414, 32-45.	2.3	37
11	4D nano-tomography of electrochemical energy devices using lab-based X-ray imaging. Nano Energy, 2018, 47, 556-565.	16.0	37
12	Virtual unrolling of spirally-wound lithium-ion cells for correlative degradation studies and predictive fault detection. Sustainable Energy and Fuels, 2019, 3, 2972-2976.	4.9	37
13	Enhanced composite plate impact damage detection and characterisation using X-Ray refraction and scattering contrast combined with ultrasonic imaging. Composites Part B: Engineering, 2020, 181, 107579.	12.0	37
14	A spinal organ of proprioception for integrated motor action feedback. Neuron, 2021, 109, 1188-1201.e7.	8.1	36
15	A Structure and Durability Comparison of Membrane Electrode Assembly Fabrication Methods: Self-Assembled Versus Hot-Pressed. Journal of the Electrochemical Society, 2018, 165, F3045-F3052.	2.9	34
16	X-ray tomography and modelling study on the mechanical behaviour and performance of metal foam flow-fields for polymer electrolyte fuel cells. International Journal of Hydrogen Energy, 2019, 44, 7583-7595.	7.1	34
17	Effect of Microstructure of Porous Transport Layer on Performance in Polymer Electrolyte Membrane Water Electrolyser. Energy Procedia, 2018, 151, 111-119.	1.8	33
18	Multiâ€Scale Imaging of Polymer Electrolyte Fuel Cells using Xâ€ray Micro―and Nanoâ€Computed Tomography, Transmission Electron Microscopy and Heliumâ€Ion Microscopy. Fuel Cells, 2019, 19, 35-42.	2.4	31

#	Article	IF	CITATIONS
19	3D Imaging of Lithium Protrusions in Solidâ€State Lithium Batteries using Xâ€Ray Computed Tomography. Advanced Functional Materials, 2021, 31, 2007564.	14.9	31
20	Correlative acoustic time-of-flight spectroscopy and X-ray imaging to investigate gas-induced delamination in lithium-ion pouch cells during thermal runaway. Journal of Power Sources, 2020, 470, 228039.	7.8	30
21	Microstructure analysis and image-based modelling of face masks for COVID-19 virus protection. Communications Materials, 2021, 2, .	6.9	30
22	Provenance and geological significance of red mud and other clastic sediments of the Mugnano cave (Montagnola Senese, Italy). International Journal of Speleology, 2012, 41, 317-328.	1.0	29
23	MicroCT optimisation for imaging fascicular anatomy in peripheral nerves. Journal of Neuroscience Methods, 2020, 338, 108652.	2.5	29
24	X-ray Phase-Contrast Radiography and Tomography with a Multiaperture Analyzer. Physical Review Letters, 2017, 118, 243902.	7.8	27
25	Environmental magnetic implications of magnetofossil occurrence during the Middle Eocene Climatic Optimum (MECO) in pelagic sediments from the equatorial Indian Ocean. Palaeogeography, Palaeoclimatology, Palaeoecology, 2016, 441, 212-222.	2.3	26
26	Threeâ€Phase Segmentation of Solid Oxide Fuel Cell Anode Materials Using Lab Based Xâ€ray Nano omputed Tomography. Fuel Cells, 2017, 17, 75-82.	2.4	26
27	Imaging fascicular organization of rat sciatic nerves with fast neural electrical impedance tomography. Nature Communications, 2020, 11, 6241.	12.8	24
28	Metabolically diverse primordial microbial communities in Earth's oldest seafloor-hydrothermal jasper. Science Advances, 2022, 8, eabm2296.	10.3	24
29	The Imaging Resolution and Knudsen Effect on the Mass Transport of Shale Gas Assisted by Multi-length Scale X-Ray Computed Tomography. Scientific Reports, 2019, 9, 19465.	3.3	22
30	Prevention of lithium-ion battery thermal runaway using polymer-substrate current collectors. Cell Reports Physical Science, 2021, 2, 100360.	5.6	22
31	Pore structure development during hydration of tricalcium silicate by X-ray nano-imaging in three dimensions. Construction and Building Materials, 2019, 200, 318-323.	7.2	21
32	Three-Dimensional Visualization of Conductive Domains in Battery Electrodes with Contrast-Enhancing Nanoparticles. ACS Applied Energy Materials, 2018, 1, 4479-4484.	5.1	20
33	Evolution with depth from detrital to authigenic smectites in sediments from AND-2A drill core (McMurdo Sound, Antarctica). Clay Minerals, 2012, 47, 481-498.	0.6	19
34	Geosources for ceramic production: The clays from the Neogene–Quaternary Albegna Basin (southern Tuscany). Applied Clay Science, 2014, 91-92, 105-116.	5.2	17
35	In-situ X-ray tomographic imaging study of gas and structural evolution in a commercial Li-ion pouch cell. Journal of Power Sources, 2022, 520, 230818.	7.8	17
36	The multiscale hierarchical structure of Heloderma suspectum osteoderms and their mechanical properties. Acta Biomaterialia, 2020, 107, 194-203.	8.3	16

#	Article	IF	CITATIONS
37	Examining the effect of the secondary flow-field on polymer electrolyte fuel cells using X-ray computed radiography and computational modelling. International Journal of Hydrogen Energy, 2019, 44, 1139-1150.	7.1	15
38	Dendritic silver self-assembly in molten-carbonate membranes for efficient carbon dioxide capture. Energy and Environmental Science, 2020, 13, 1766-1775.	30.8	15
39	Correlation of X-ray diffraction signatures of breast tissue and their histopathological classification. Scientific Reports, 2017, 7, 12998.	3.3	14
40	Multimodal Phase-Based X-Ray Microtomography with Nonmicrofocal Laboratory Sources. Physical Review Applied, 2017, 8, .	3.8	14
41	Thermally Driven SOFC Degradation in 4D: Part I. Microscale. Journal of the Electrochemical Society, 2018, 165, F921-F931.	2.9	14
42	Xâ€ray Nanoâ€computed Tomography of Electrochemical Conversion in Lithiumâ€ion Battery. ChemSusChem, 2019, 12, 3550-3561.	6.8	14
43	Evidence of structural cavities in 3D printed acetabular cups for total hip arthroplasty. Journal of Biomedical Materials Research - Part B Applied Biomaterials, 2020, 108, 1779-1789.	3.4	14
44	Three dimensional characterisation of chromatography bead internal structure using X-ray computed tomography and focused ion beam microscopy. Journal of Chromatography A, 2018, 1566, 79-88.	3.7	13
45	Thermally Driven SOFC Degradation in 4D: Part II. Macroscale. Journal of the Electrochemical Society, 2018, 165, F932-F941.	2.9	12
46	Anomalous transport of colloids in heterogeneous porous media: A multi-scale statistical theory. Journal of Colloid and Interface Science, 2022, 617, 94-105.	9.4	11
47	A Multiscale Xâ€Ray Tomography Study of the Cycledâ€Induced Degradation in Magnesium–Sulfur Batteries. Small Methods, 2021, 5, e2001193.	8.6	10
48	Clay minerals in cave sediments and terra rossa soils in the Montagnola Senese karst massif (Italy). Geological Quarterly, 2013, 57, .	0.2	10
49	Miocene Glacial Dynamics Recorded by Variations in Magnetic Properties in the ANDRILLâ€2A Drill Core. Journal of Geophysical Research: Solid Earth, 2019, 124, 2297-2312.	3.4	9
50	Ultra high-resolution biomechanics suggest that substructures within insect mechanosensors decisively affect their sensitivity. Journal of the Royal Society Interface, 2022, 19, 20220102.	3.4	9
51	Improved X-ray computed tomography reconstruction of the largest fragment of the Antikythera Mechanism, an ancient Greek astronomical calculator. PLoS ONE, 2018, 13, e0207430.	2.5	8
52	Packed bed compression visualisation and flow simulation using an erosion-dilation approach. Journal of Chromatography A, 2020, 1611, 460601.	3.7	7
53	Microporous Biodegradable Films Promote Therapeutic Angiogenesis. Advanced Healthcare Materials, 2020, 9, e2000806.	7.6	7
54	Rapid Preparation of Geometrically Optimal Battery Electrode Samples for Nano Scale X-ray Characterisation. Journal of the Electrochemical Society, 2020, 167, 060512.	2.9	7

FRANCESCO IACOVIELLO

#	Article	IF	CITATIONS
55	An open-source platform for 3D-printed redox flow battery test cells. Sustainable Energy and Fuels, 2022, 6, 1529-1540.	4.9	7
56	A multi-method assessment of 3D printed micromorphological osteological features. International Journal of Legal Medicine, 2022, 136, 1391-1406.	2.2	6
57	Evaluating microstructure evolution in an SOFC electrode using digital volume correlation. Sustainable Energy and Fuels, 2018, 2, 2625-2635.	4.9	4
58	Motion-enhancement assisted digital image correlation of lithium-ion batteries during lithiation. Journal of Power Sources, 2022, 527, 231150.	7.8	4
59	In situ x-ray computed tomography of zinc–air primary cells during discharge: correlating discharge rate to anode morphology. JPhys Materials, 2022, 5, 014001.	4.2	4
60	The Time-Dependent Role of Bisphosphonates on Atherosclerotic Plaque Calcification. Journal of Cardiovascular Development and Disease, 2022, 9, 168.	1.6	3
61	Alteration of volcanic deposits in the ANDRILL AND-1B core: Influence of paleodeposition, eruptive style, and magmatic composition. , 2013, 9, 275-286.		2
62	Early Miocene Antarctic glacial history: new insights from heavy mineral analysis from ANDRILL AND-2A drill core sediments. International Journal of Earth Sciences, 2015, 104, 853-872.	1.8	2
63	High-resolution imaging of depth filter structures using X-ray computed tomography. Journal of Materials Science, 2021, 56, 15313.	3.7	1
64	Liposome Sterile Filtration Characterization via X-ray Computed Tomography and Confocal Microscopy. Membranes, 2021, 11, 905.	3.0	1
65	Fascicular Organisation and Neuroanatomy of the Porcine and Human Vagus Nerves: Allowing for Spatially Selective Vagus Nerve Stimulation. FASEB Journal, 2022, 36, .	0.5	1
66	Use of Photon Scattering Interactions in Diagnosis and Treatment of Disease. , 2018, , 135-158.		0